Rapid self-healing hydrogels

Ameya Phadke[a], Chao Zhang[a], Bedri Arman[b], Cheng-Chih Hsu[c], Raghunath A. Mashelkar[d,1], Ashish K. Lele[d], Michael J. Tauber[c], Gaurav Arya[b], and Shyni Varghese[a,1]

[a]Departments of Bioengineering, [b]NanoEngineering, and [c]Chemistry and Biochemistry, University of California at San Diego, La Jolla, CA 92093; and [d]National Chemical Laboratory, Pune 411008, India

Contributed by Raghunath A. Mashelkar, January 23, 2012 (sent for review December 2, 2011)

Synthetic materials that are capable of autonomous healing upon damage are being developed at a rapid pace because of their many potential applications. Despite these advancements, achieving self-healing in permanently cross-linked hydrogels has remained elusive because of the presence of water and irreversible cross-links. Here, we demonstrate that permanently cross-linked hydrogels can be engineered to exhibit self-healing in an aqueous environment. We achieve this feature by arming the hydrogel network with flexible-pendant side chains carrying an optimal balance of hydrophilic and hydrophobic moieties that allows the side chains to mediate hydrogen bonds across the hydrogel interfaces with minimal steric hindrance and hydrophobic collapse. The self-healing reported here is rapid, occurring within seconds of the insertion of a crack into the hydrogel or juxtaposition of two separate hydrogel pieces. The healing is reversible and can be switched on and off via changes in pH, allowing external control over the healing process. Moreover, the hydrogels can sustain multiple cycles of healing and separation without compromising their mechanical properties and healing kinetics. Beyond revealing how secondary interactions could be harnessed to introduce new functions to chemically cross-linked polymeric systems, we also demonstrate various potential applications of such easy-to-synthesize, smart, self-healing hydrogels.

biomimetic materials | hydrophobicity | smart materials | molecular dynamics | adhesives

Recent years have witnessed an increasing interest in the development of "smart" materials that can sense changes in their environment and can accordingly adapt their properties and function, similar to living systems. Over the last decade, we have discovered and demonstrated a class of smart hydrogels that exhibit unique biomimicking functions: thermoresponsive volume phase transitions similar to sea cucumbers (1), self-organization into core-shell hollow structures similar to coconuts (2), shape memory as exhibited by living organisms (2), and metal ion-mediated cementing similar to marine mussels (3). A common thread connecting these smart hydrogels is their possession of a unique balance of hydrophilic and hydrophobic interactions that endows the hydrogels with the biomimicking properties described above. In this study, we demonstrate how this concept of balancing hydrophilic and hydrophobic forces could be exploited to design chemically cross-linked hydrogels with self-healing abilities.

Indeed, materials capable of autonomous healing upon damage have numerous potential applications (4–6). So far, self-healing has been demonstrated in linear polymers (7), supramolecular networks (8, 9), dendrimer-clay systems (10), metal ion-polymer systems (11, 12), and multicomponent systems (13–17). Whereas multicomponent thermosetting systems harness the ability of embedded chemical agents to repair cracks, supramolecular networks and noncovalent hydrogels employ secondary interactions such as hydrogen bonding, ionic interactions, and hydrophobic association for healing. However, self-healing of permanently cross-linked systems such as hydrogels has remained elusive because of the presence of water and irreversible chemical cross-links, in spite of the many applications in biomedical sciences that such aqueous healing systems could offer.

We propose that self-healing could be achieved in hydrogels by decorating the polymer network with dangling hydrocarbon side chains containing polar functional groups that would mediate hydrogen bonding across two separate hydrogel pieces or across a rupture in the hydrogel. However, to achieve efficient and robust healing, the side chains must be sufficiently long and flexible, and the network sufficiently deformable, to make the functional groups across the interface accessible to each other beyond the corrugation of the interface. At the same time, the side chains should be short enough to minimize steric hindrance of the interacting functional groups and to prevent hydrophobic collapse of the side chains. In effect, the side chains should possess an optimal balance of hydrophobic and hydrophilic moieties.

We have previously shown that polymer hydrogels formulated from acryloyl-6-aminocaproic acid (A6ACA) precursors possess an optimal balance of hydrophobic and hydrophilic interactions that allows its side chains to bind to exogenous metal ions (2, 11) and to extracellular proteins (18). The above finding suggests that the elastomeric properties of the A6ACA hydrogels along with their flexible side chains might be able to mediate hydrogen bonding across two hydrogel interfaces through the amide and carboxylic functional groups. Consequently, we hypothesize that hydrogels synthesized from such precursors might exhibit self-healing in an aqueous environment in spite of their irreversible cross-linked architecture.

Results and Discussion

A6ACA Hydrogels Demonstrate Rapid and Robust Self-Healing. The A6ACA hydrogels were synthesized as described in *Materials and Methods* (Fig. 1*A*, Figs. S1 and S2, and *SI Text*). We observed that two lightly cross-linked A6ACA hydrogels weld rapidly to each other within 2 s when brought in contact in low-pH aqueous solution (pH $\leq$ 3) (Fig. 1*B* and Movie S1), thus supporting our hypothesis. The healed hydrogels exhibit a strong interface capable of withstanding their own weight(s), repeated stretching, and exposure to boiling water (Fig. 1*C* and Movies S1 and S2). The healed samples are able to sustain large deformations and recover their size and shape when the stress is released (Movie S2). This pH-mediated healing is also reversible: Two healed hydrogels separate when exposed to high pH (Fig. 1*D*). The separated hydrogels are able to reheal upon reintroduction into a low-pH environment (Fig. 1*D*). The cycle of healing, separation, and rehealing is repeated many (>12) times without hysteresis; the healing occurs on the same timescale and with comparable weld-line strength as that of the original hydrogels.

Role of Hydrogen Bonding in Self-Healing. To confirm that the observed healing in A6ACA hydrogels is mediated through hydro-

Author contributions: A.P., G.A., and S.V. designed research; A.P., C.Z., B.A., C.-C.H., M.J.T., and S.V. performed research; A.P., C.Z., B.A., C.-C.H., R.A.M., A.K.L., M.J.T., G.A., and S.V. analyzed data; and A.P., C.Z., B.A., R.A.M., A.K.L., M.J.T., G.A., and S.V. wrote the paper.

The authors declare no conflict of interest.

[1]To whom correspondence may be addressed. E-mail: svarghese@ucsd.edu or ram@ncl.res.in.

This article contains supporting information online at www.pnas.org/lookup/suppl/doi:10.1073/pnas.1201122109/-/DCSupplemental.

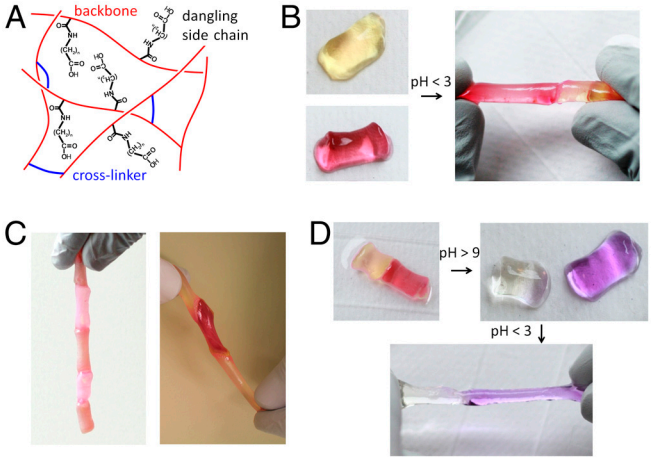

Fig. 1. Self-healing hydrogels. (*A*) Schematic illustration of the structure of self-healing A6ACA hydrogels containing dangling side chains terminating with a carboxyl group. (*B*) Deprotonated cylindrical hydrogels at pH 7.4 (*Left*) heal in low-pH solution (pH ≤ 3) (*Right*). The hydrogels are dyed yellow and maroon to allow for easily distinguished interface. (*C*) Healed hydrogels carrying their own weight(s) (*Left*) and being stretched manually (*Right*) illustrate the weld-line strength. (*D*) The healed hydrogels at low pH (*Left*) separate after exposure to a high-pH solution (with pH > 9) (*Right*). The change in color is due to the reaction of the dyes with the NaOH solution. (*Lower*) The separated hydrogels in (*Upper*) reheal upon exposure to acidic solution (pH < 3).

gen bonding, we immersed the healed hydrogels into a urea solution, which is known to disrupt hydrogen bonds (19). As expected, the immersion results in the separation of the two hydrogels at their interface (Fig. S3).

The role of hydrogen bonding is further analyzed by using FTIR–attenuated total reflectance (ATR) and Raman spectroscopy (Fig. 2*A* and *B*, Table S1, and *SI Text*). The hydrogen-bonded terminal carboxylic-acid group is evident from the Raman band at 1,714 cm^{-1} and IR band at 1,704 cm^{-1} observed in healed hydrogels (Fig. 2 *A* and *B*). The spectroscopic analyses of the healed hydrogels suggest two different types of hydrogen bonding across the interface. First, the spectral features support direct interaction of carboxyl groups with the amide groups of the opposing pendant side chain in an interleaved configuration (Fig. 2*C*). In particular, the prominent IR band at 1,627 cm^{-1} and the corresponding weak Raman band at 1,624 cm^{-1}, assigned to the amide I mode (majority C = O stretch, some C–N stretch), indicate the presence of strongly hydrogen-bonded amide groups (20, 21). Second, the spectral features suggest a smaller fraction of carboxyl groups interacting with the opposing carboxyl groups in a face-on configuration (22) (Fig. 2*C*). Consistent with this configuration, we observe evidence of a small population of amide groups having similar amide I band intensity for healed and unhealed hydrogels, suggesting similarity in their H-bond environment irrespective of their protonation state. We have confirmed through molecular modeling that the interleaved and face-on configurations are sterically feasible (Fig. S4).

The above analyses suggest an intriguing mechanism for the observed pH-mediated self-healing. At low pH, the terminal-carboxyl groups are mostly protonated, which allows them to form hydrogen bonds with other terminal-carboxyl groups or amide groups across the interface, thereby allowing the hydrogels to weld (Fig. 2*C*). At pH above their pK_a (4.4 for 6-aminocaproic acid, the parent amino acid from which the A6ACA monomer is synthesized) (23), the A6ACA carboxyl groups are deprotonated and exhibit significant electrostatic repulsion, which prevents hydrogen bonding (Fig. 2*D*). We also find that the healing ability of the hydrogels diminishes with prolonged exposure to low-pH environment prior to healing, but can be restored by immersing the hydrogels in a high-pH environment followed by reintroduction into a low-pH environment. The prolonged exposure of the hydrogels to a low-pH environment could lead to intramolecular hydrogen bonding, which decreases their availability to form intermolecular hydrogen bonds across the interface.

Mechanical Characterization of Healed Hydrogels. A study of the temporal dependence of the healing indicates an increase in weld-line strength with time over a period of 10 s to 24 h (Fig. 3*A*). Hydrogels healed for 10 s withstand more than 2.04 ± 0.07 kPa stresses whereas those healed for over 5 min fail upon an application of 2.7 ± 0.2 kPa stress. In both cases, the hydrogels always rupture in the bulk region, whereas the welded interface remains intact (Fig. S5*A*), indicating a strongly healed interface. The low mechanical strength of the bulk region is attributed to its inherent soft nature compared to the surfaces that are in contact with the low-pH solution, as schematically shown in Fig. 2*E*. Therefore, the interfacial region toughens as a result of protonation of the carboxyl groups and subsequent increase in their hydrogen bonding. In contrast, the interior bulk regions remain soft because protons cannot diffuse into the polymer network within the experimental timescales. However, after extended exposure (approximately 24 h) to low-pH solution, the hydrogels become capable of withstanding large stresses (35 ± 3 kPa) and break at the interface. Moreover, the 24-h healed hydrogels become opaque because of protonation-induced hydrophobic collapse of the polymer chains (Fig. S5*B*).

Fig. 3*B* shows that the maximum stress required to break 24-h healed hydrogels is 66 ± 7% of that of single hydrogel pieces of similar dimensions treated under identical conditions. The fracture stress in healed hydrogels is lower than in single hydrogels because failure in healed hydrogels involves only breakage of intermolecular hydrogen bonds across the interface whereas failure in single hydrogels involves breakage of both covalent bonds and intramolecular hydrogen bonds. The ratio of the elastic moduli, $E_{healed}/E_{single} = 1.1 \pm 0.5$ (where E_{healed} and E_{single} represent the elastic moduli of the 24-h healed and unhealed hydrogels, respectively) indicates little change in the stiffness of the hydrogels after healing.

Effect of Cross-Link Density and Side- Chain Length on Healing. To determine the effect of cross-link density on healing, A6ACA hydrogels with varying cross-linker content were prepared (Fig. S2*C*). The self-healing depends strongly on the extent of cross-linking and thereby the swelling behavior of the hydrogels. Specifically, the interfacial strength of healed hydrogels decreases with increasing cross-linker content (Fig. 3*C*). The reduction in healing efficiency could be attributed to either the restricted mobility of the side chains or to the decrease in the compliance of the hydrogel with increasing cross-linking, both of which could impede the formation of hydrogen bonds across the interface. The latter effect, however, seems to be the more likely explanation given that the hydrogel still exhibits significant swelling at the high cross-link densities, indicating that the molecular pores might be considerably larger than the side chains and thus do not interfere significantly with the side-chain mobility.

Next, we investigated the effect of pendant side-chain length on healing by synthesizing hydrogels with similar cross-linker content but varying side-chain lengths, containing 1–10 methylene groups, terminating with a carboxyl group (Fig. S6*A*). Hydrogels with side chains containing 1–3 and 10 methylene groups do not exhibit any healing and those containing 7 methylene groups [*N*-acryloyl 8-aminocaprylic acid (A8ACA)] show weak healing (Fig. S6*B*). The A8ACA hydrogels required more than 5 min to heal, and the healed hydrogels could be separated easily by a small stress (0.267 ± 0.008 kPa). Thus, interestingly, the healing ability depends nonmonotonically on the side-chain length.

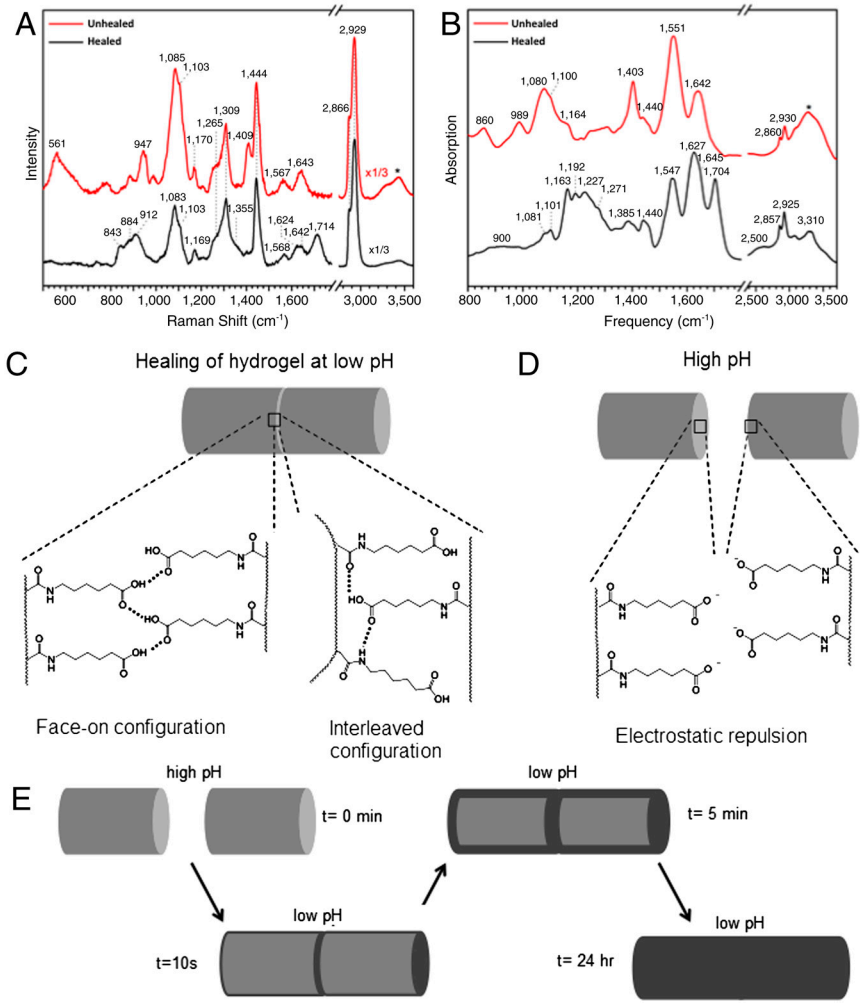

Fig. 2. Mechanism of self-healing in A6ACA hydrogels. Raman (*A*) and FTIR–ATR (*B*) spectroscopy of healed (low pH) and unhealed (high pH) hydrogels demonstrating the presence of multiple types of hydrogen-bonded carboxyl groups. (*C*) Deduced molecular structures of pendant side chains in the face-on and interleaved hydrogen-bonding configurations responsible for the healing at low pH. (*D*) Structure of the pendant side chains in the unhealed hydrogels at high pH. At high pH, the carboxyl groups become deprotonated, leading to strong electrostatic repulsion between the apposing side chains, thus preventing healing. (*E*) Schematic explanation for why the healed hydrogels exhibit a mechanically stronger weld line compared to the bulk after healing for small timescales, and vice versa at very long times. Darker gray represents the toughened regions of the hydrogels due to protonation. The lighter gray represents the deprotonated (softer) regions of the hydrogels, which protonates and toughens with increasing exposure to low-pH solution.

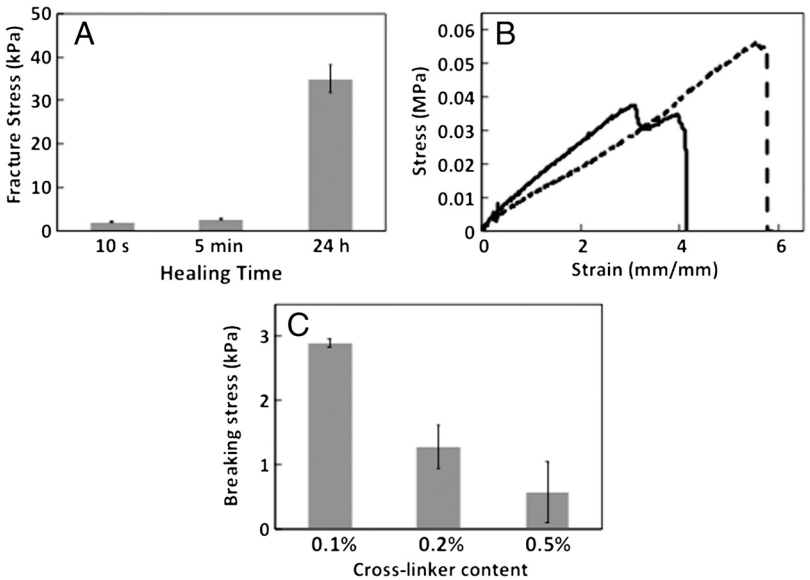

Fig. 3. Characterization of healing and healed hydrogels. (*A*) Effect of healing time on fracture stress. (*B*) Stress–strain curve, comparing tensile properties of 24-h healed gels with a single, unhealed hydrogel at identical conditions. The solid and dashed lines represent data from healed and unhealed hydrogels, respectively. (*C*) Fracture stress as a function of the extent of cross-linking for hydrogels containing 0.1%, 0.2%, and 0.5% of cross-linker (*N*, *N*′-methylenebisacrylamide) content. Error bars in *A* and *C* represent the standard deviation ($n = 3$).

The low healing ability of hydrogels with short side chains could be attributed to the limited "reach" of the carboxyl groups in mediating hydrogen bonds with functional groups across the interface, especially given that the hydrogel surfaces are likely corrugated. As the side chains become longer, the terminal-carboxyl groups become more flexible and increase their reach for hydrogen bonding, especially with the internal amide groups of the apposing hydrogel. When the side chains become too long, they begin to pose a larger steric hindrance to the interactions between the carboxyl and amide groups. In addition, the long side chains tend to aggregate and collapse because of increased hydrophobic interactions. This effect can be gleaned from the water solubility of carboxylic acids of varying hydrocarbon chain lengths (24) (Fig. 4*A*); i.e., chains containing more than six CH_2 groups become insoluble in water at concentrations similar to the effective concentration of side chains present in the hydrogel (approximately 0.02 M for A6ACA). Both the steric hindrance and hydrophobic collapse reduce the accessibility of the amide groups, leading to a reduction in the healing efficiency.

To confirm the suggested decrease in the accessibility of the amide groups with increasing chain length, we have conducted molecular dynamics simulations of A6ACA, A8ACA, and *N*-acryloyl 11-aminoundecanoic acid (A11AUA) hydrogel networks in an aqueous medium (Fig. 4*B*). We have quantified the accessibility of the terminal-carboxyl and internal-amide groups in terms of the average number of hydrogen bonds they form with the surrounding water molecules during the simulation (Fig. 4*C*). Our simulations demonstrate a substantial decrease in the accessibility of the amide groups with increasing side-chain length, whereas the accessibility of the carboxyl groups changes only slightly with the chain length. Fig. 4*D* shows representative configurations of the A6ACA and A11AUA hydrogel within one unit cell obtained from our simulations. The configurations are shown in a solvent excluded surface representation to illustrate the reduction in the accessibility of the amide groups (shown in blue) in going from the short to long side chains. The correlation between amide groups accessibility and healing ability for A6ACA, A8ACA, and A11AUA hydrogel provides further support for the dominant role played by the interleaved hydrogen bonding configuration in self-healing as evidenced from spectroscopic analyses.

The observed dependence of healing on the side-chain length thus confirms our hypothesis that self-healing is best exhibited by hydrogels possessing a balance of hydrophobic and hydrophilic interactions. Interestingly, this requirement along with that for flexible side chains to mediate hydrogen bonding across the interface explains why many polymeric systems including protein hydrogels do not exhibit robust self-healing despite their possessing amide and carboxylic functional groups.

Demonstrated Applications of Self-Healing Hydrogels. The self-healing hydrogels developed here—which remain healed over a wide range of temperatures, light conditions, and humidity—could have numerous applications in medicine, environmental science, and industry. We have explored several of such applications.

We first investigated the application of these hydrogels as self-repairing coatings and sealants. We coated various surfaces with A6ACA hydrogels and mechanically damaged the coatings with 300-μm-wide cracks (Fig. 5*A*). The coatings healed the imparted crack within seconds upon exposure to low-pH buffers (Fig. 5*B*). Because this healing only requires initial contact, one can achieve repair by simply spraying the cracks with a low-pH buffer. We found that these hydrogels could adhere to various plastics like polypropylene and polystyrene even in their hydrated state; this is likely because of hydrophobic interactions (Fig. 5*C*). This finding, in conjunction with the observed rapid pH-dependent healing, suggests that these hydrogels could be used as sealants for vessels containing corrosive acids. As a proof-of-concept, we created a hole in a polypropylene container, then coated it with A6ACA hydrogel, and finally poured hydrochloric acid into it. The hydrogel instantly sealed the hole and prevented any leakage of the acid (Fig. 5*D*).

We have also investigated the application of A6ACA hydrogels as tissue adhesives, with an emphasis on gastric tissue that is typically exposed to low pH, an environment in which the hydrogels can heal easily. The mucoadhesive ability of A6ACA hydrogels was investigated by using fresh gastric mucosa of rabbits. Fig. 5*E* demonstrates that A6ACA hydrogels adhere well to the gastric mucosa and that the adhesion is strong enough to support the weight of the hydrogel. Thus, A6ACA hydrogels could indeed be used as tissue adhesives for stomach perforations, where the lightly cross-linked hydrogels could be injected to prevent leakage of gastric acids. In addition, such mucoadhesive hydrogels could also be employed for drug delivery if the hydrogels could store and release bioactive molecules without compromising their ac-

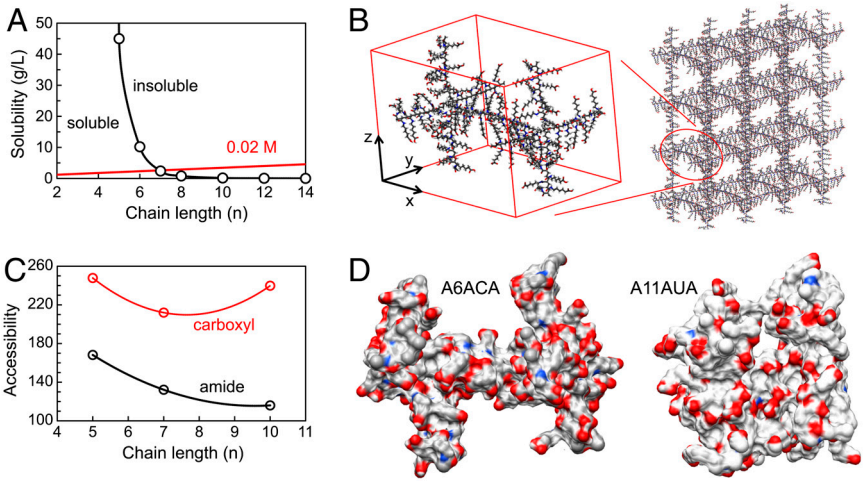

Fig. 4. Effect of side-chain length on the accessibility of functional groups. (*A*) Solubility of carboxylic acids of varying hydrocarbon chain lengths in water (black circles). Dashed red line indicates the density of carboxyl groups present in the hydrogels. (*B*) Molecular dynamics simulations setup for A6ACA network. A nine-arm motif of the network (*Left*) is used to create the 3D network structure (*Right*) via periodic boundary conditions. (*C*) Computed accessibilities of the amide and carboxyl groups in the A6ACA, A8ACA, and A11AUA hydrogels. (*D*) Representative configuration of the A6ACA and A11AUA network obtained from molecular dynamics simulations, shown in terms of solvent excluded surface, illustrating the higher accessibility of the amide groups in the former network. Blue, red, light gray, and white colors correspond to the surfaces of nitrogen, oxygen, carbon, and hydrogen, respectively. Chain length *n* in *A* and *C* represent number of CH_2 groups in the carboxylic acids and side chains, respectively.

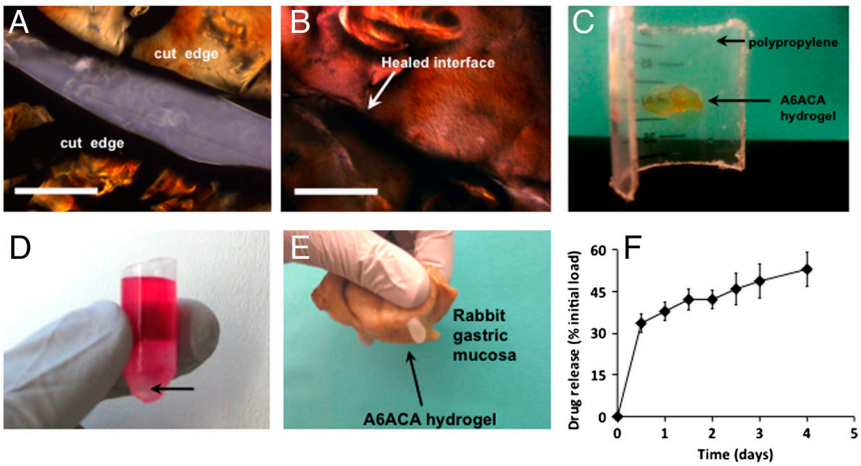

Fig. 5. Applications of self-healing A6ACA hydrogels. The rupture site within the A6ACA coating on a polystyrene surface (*A*) before and (*B*) after healing. The coating was colored using a dye for easy visualization and the observed color change after healing is caused by its exposure to low-pH buffer. (Scale bars: 500 μm.) (*C*) Adhesion of A6ACA hydrogels to a poly(propylene) surface. (*D*) Polypropylene container holding acid solution after sealing the hole with A6ACA hydrogel. The arrow indicates the sealed site. (*E*) Adhesion of A6ACA hydrogels to rabbit gastric mucosa. (*F*) Cumulative tetracycline release from A6ACA hydrogels plotted as a function of time. Error bars represent standard deviation ($n = 4$).

tivity. To explore the potential of A6ACA hydrogels as drug carriers, we used tetracycline as a model system. The tetracycline-loaded hydrogels were exposed to a simulated gastric acid environment (pH 1.5) and the drug-release profile was evaluated. Tetracycline was released at a constant rate for 4 d after the initial bolus release (Fig. 5*F*).

Finally, the ability of these hydrogels to fuse could also allow for the development of soft structures with complex architectures (Fig. S7). Such structures could find applications as soft actuators and in robotic devices.

In summary, we have demonstrated that self-healing can be achieved in chemically cross-linked systems through introduction of pendant side chains possessing an optimal balance of hydrophilic and hydrophobic moieties, using A6ACA as a model system. The self-healing hydrogels described here represent an exciting class of smart, easy-to-synthesize materials with widespread potential applications in biology, medicine, and engineering.

Materials and Methods

Synthesis of Acryloyl Amino Acid Monomers. The monomers were synthesized and characterized as described elsewhere (18). See *SI Text* for more details.

Synthesis and Characterization of Hydrogels. Hydrogels were prepared by free radical polymerization. See *SI Text* for more details on synthesis and characterization of various hydrogels.

Healing of the Hydrogels. Healing of hydrogels was carried out in different buffer solutions with pH ranging from 0.3–7.4. Specifically, we used 0.5 M hydrochloric acid (pH 0.3), 1× phosphate-buffered saline (pH 7.4), and other buffer solutions, as detailed in Table S2. The hydrogel samples were brought into contact with each other without application of any external force. For ease of visualization, the hydrogels were dyed yellow and maroon by soaking them in PBS containing 0.5% (vol/vol) methyl red indicator and approximately 0.002% (wt/vol) alizarin red S, respectively.

Mechanical Characterization. Butt-welded hydrogels were used for mechanical measurements. To determine the interfacial strength of hydrogels healed for 10 s and 5 min, we used a custom-designed approach where known weights were applied to healed hydrogels and the resulting engineering stress required to break the healed hydrogels was calculated. The mechanical properties of 24-h healed hydrogels were determined using an Instron 3342 Universal Testing System (Instron) equipped with a Model 2519-104 force transducer. A load cell of 450N was fitted to the instrument and the tensile tests were done at a cross-head speed of 15 mm/ min. The data acquisition and processing were performed with BlueHill software. The tensile modulus was determined by calculating the slope of a linear region of stress–strain curve, whereas the fracture stress was determined from the peak of the curve.

Reversibility of Healing. Cylindrical hydrogels were healed via butt welding, as described above, and then immersed in 1 M NaOH (pH 14) for 10 min for separation. The separated hydrogels were then briefly rinsed in PBS to remove excess NaOH and reintroduced into an acidic solution (pH 0.3) and healed by maintaining the surfaces in contact for less than 5 s. These rehealed hydrogels were then reintroduced into 1 M NaOH solution for separation. This cycle of healing–separation–rehealing was performed more than 12 times to test the reversibility of healing. Separation of healed hydrogels was also examined in a standard buffer solution of pH 10 (Fisher Scientific, Inc.), and it was found to be at a slower rate compared to those separated in pH-14 buffer.

Stability of Healed Hydrogels in Water and Effect of Temperature. The completely healed hydrogels were immersed in deionized (DI) water for more than a month to determine their stability at ambient temperature. To determine the effect of temperature on the stability, the healed hydrogels were immersed in boiling water at 100 °C for 1 h.

Effect of Urea on Healing Efficacy. To investigate the contribution of hydrogen bonding on healing, the butt-welded hydrogels were immersed in excess of a 30% (wt/vol) solution of urea in DI water. Another healed hydrogel immersed in DI water was used as the control.

FTIR–ATR and Raman Spectroscopy. Spectroscopic analysis was carried out on loosely cross-linked A6ACA hydrogels that were healed in 0.5 M HCl for 24 h, along with unhealed hydrogels (pH approximately 7.4) for comparison. The healed and unhealed hydrogels were dried for 24 h at 37 °C prior to performing Raman and FTIR–ATR spectroscopy to minimize interference of hydrogen-bonded water molecules. The FTIR spectra from 4,400 to 600 cm^{-1} were acquired with a Perkin Elmer Spectrum RX Fourier transform infrared spectrometer. Samples were placed on the diamond window of a PIKE MIRacle ATR attachment. Each reported spectrum is the average of four scans, and the resolution is 2 cm^{-1}. Raman spectroscopy was performed with a home-built Raman microscope system. A mixed-gas Kr-Ar ion laser (Coherent Innova 70C) provided continuous-wave excitation at 514.5 nm. The beam was sent through a 514.5-nm interference filter (Semrock) and directed into a modified fluorescence alignment port of a Zeiss Axio Imager A1m upright microscope. A broadband beam splitter (Edmund Optics) directed a small portion (approximately 10%) of the beam downward to the entrance aperture of a 50× objective. The power at the sample was 5.2 mW. Back-scattered light was collected and collimated with the same objective, filtered with a 514.5-nm edge filter (Semrock), and focused on the entrance slit of a 0.32-m focal length spectrograph (Horiba Jobin Yvon; iHR-320). Raman scattered light was dispersed with a 1,200 grooves/mm-ruled grating and detected by a thermoelectrically cooled open-electrode CCD detector (Horiba Jobin Yvon Synapse). Wavelength calibration was performed using known lines of Hg/Ar and Ne

lamps for windows centered at 550 and 610 nm, respectively. See *SI Text* for more details.

Determination of Steric Feasibility of Configurations. We sought to determine whether the face-on and interleaved configurations were sterically feasible. As a model system, we used five-unit oligomers of A6ACA (Fig. S4*A*). Two such oligomers were brought together and an energy minimization was performed using ChemBio3D Ultra 12.0 (CambridgeSoft) (Fig. S4*B*). Both face-on and interleaved species were observed in the resultant configurations (Fig. S4*B*), indicating that both types of configurations are sterically feasible.

Molecular Dynamics Simulations of Hydrogel Networks. To investigate the effect of side-chain length on healing efficiency, we performed molecular dynamics simulations of hydrogel networks built from A6ACA, A8ACA, and A11AUA monomers having side chains of lengths 5, 7, and 10 CH_2 groups, respectively. A nine-arm hydrogel motif was placed inside the simulation box along with water molecules (Fig. 4*B*, *Left*) and replicated via periodic boundary conditions to yield the desired hydrogel network (Fig. 4*B*, *Right*). A gap in the $\pm x$ direction prevented continuity of the network along the x direction and allowed the creation of a hydrogel–water interface in between periodic images of the network. The accessibility of the amide and carboxyl groups was quantified in terms of the number of hydrogen bonds they form with the water molecules. We hypothesize that the accessibility of the functional groups for interacting with water molecules is a good measure for their accessibility for interacting with functional groups from the apposing hydrogel surface. See *SI Text* for more details.

A6ACA Hydrogels as Self-Healing Coating. A6ACA hydrogels were swollen in a 0.01% solution of methyl red in PBS, to gain contrast between the coating and the surface. Polystyrene surfaces were coated with the hydrogels by drying at 37 °C for 12 h. A 300-μm-wide scratch was made in the coating surface using a surgical scalpel and imaged using bright field microscopy (Axio Observer A1; Carl Zeiss). The scratch site was briefly hydrated for 60 s with 50 μL DI water after which the excess water was removed and the site was treated with 100 μL of 0.1 M HCl. The cut edges facing each other were then reimaged after 5 min.

Adhesion of A6ACA Hydrogels to Plastics. A6ACA hydrogels were swollen in PBS for 4 h. The swollen hydrogel was found to adhere to polypropylene and polystyrene surfaces within 15–20 s upon spraying with pH-0.3 solution at the hydrogel-plastic interface.

A6ACA Hydrogels for Sealing Acid Leakages. The conical bottom portion of a 2-mL centrifuge tube (Eppendorf) was cut out to create a hole, measuring approximately 1 cm in diameter. The hole was plugged using PBS-swollen A6ACA hydrogels. This sealed conical tube was then filled with 1 mL of 0.5 M HCl (with 0.5% added methyl red, to make the solution pink for ease of visualization) and photographed to show lack of any leak.

A6ACA Hydrogels as Mucoadhesive Polymer. Stomach tissues were resected from freshly killed New Zealand white rabbits and carefully rinsed with PBS to remove residual food material. After cleaning, the tissues were maintained in PBS and used for the experiments the same day. To investigate mucoadhesiveness of A6ACA hydrogels, hydrogels were first maintained in contact with inner gastric lining under immersion in simulated gastric acid [HCl-KCl buffer of pH 1.5 containing 54.7% (by volume) 0.2 M KCl and 45.3% 0.2 M HCl] for 20 min and then photographed.

A6ACA Hydrogel as a Drug Carrier. A solution containing 0.5 mg/mL tetracycline (50×) in PBS was prepared from a stock solution of tetracycline (1,000×, 10 mg/mL in 70% ethanol). As-synthesized A6ACA hydrogels ($n = 4$) were loaded with tetracycline by placing them in this solution for 24 h. Based on the known swelling ratio of A6ACA hydrogels in PBS, the total tetracycline load was calculated for each hydrogel. The hydrogels were then immersed in 40 mL of simulated gastric fluid (pH 1.5) and placed on a shaker at 150 rpm. Every 12 h, 4 mL of the immersion solutions were collected and replaced with 4 mL of fresh buffer. The released tetracycline in the collected solutions was measured spectrophotometrically at 270 nm. The total tetracycline release (expressed as percentage of total tetracycline load, calculated from swelling ratio of hydrogels) was calculated for each time point and averaged across the replicates.

Synthesis of Complex Structures Using Healing Ability of A6ACA Hydrogels. Cylindrical A6ACA hydrogels were swollen in PBS containing 0.5% methyl red or approximately 0.002% alizarin red S, respectively. Using the yellow pieces (swollen in methyl red), hydrogels were healed to form the letter "U" with 0.5 mL HCl. Following this, the healed U was separated into the different pieces using 1 N NaOH. These pieces were then rehealed to form the letter "S." Using the pieces swollen in the alizarin red S (appearing maroon in color), a similar procedure was carried to form the letters "C" and "D." A combination of yellow- and maroon-dyed pieces was also healed to form a humanoid figure.

ACKNOWLEDGMENTS. The authors gratefully acknowledge Dr. Robert Pomeroy for assistance with FTIR–ATR analysis; Dr. Mark A Meyers, Chung-Ting Wei, Marco Maruggi, and Rui Yang for their help with mechanical measurements; Dr. Srinivas Alla for discussions on molecular modeling; Dr. Koichi Masuda for providing the rabbit stomachs; and Mr. Anthony Mrse for his assistance with ^{13}C NMR data acquisition. A.P. acknowledges financial assistance from the Jacobs Fellowship at the University of California, San Diego. We also thank the California Institute of Regenerative Medicine (RN2-00945) for financial support.

1. Varghese S, Lele AK, Mashelkar RA (2000) Designing new thermoreversible gels by molecular tailoring of hydrophilic-hydrophobic interactions. *J Chem Phys* 112:3063–3070.
2. Varghese S, Lele AK, Srinivas D, Sastry M, Mashelkar RA (2001) Novel macroscopic self-organization in polymer gels. *Adv Mater* 13:1544–1548.
3. Varghese S, Lele AK, Mashelkar R (2006) Metal-ion-medaited healing of gels. *J Polym Sci A1* 44:666–670.
4. Wojtecki RJ, Meador MA, Rowan SJ (2011) Using the dynamic bond to access macroscopically responsive structurally dynamic polymers. *Nat Mater* 10:14–27.
5. Hager MD, Greil P, Leyens C, van der Zwaag S, Schubert US (2010) Self-healing materials. *Adv Mater* 22:5424–5430.
6. Messersmith PB, Lee H, Dellatore SM, Miller WM (2007) Mussel-inspired surface chemistry for multifunctional coatings. *Science* 318:426–430.
7. de Gennes PG (1971) Reptation of polymer chain in the presence of fixed obstacles. *J Chem Phys* 55:572–579.
8. Cordier P, Tournilhac F, Soulie-Ziakovic C, Leibler L (2008) Self-healing and thermoreversible rubber from supramolecular assembly. *Nature* 451:977–980.
9. Burnworth M, et al. (2011) Optically healable supramolecular polymers. *Nature* 472:334–337.
10. Wang Q, et al. (2010) High-water-content mouldable hydrogels by mixing clay and a dendritic molecular binder. *Nature* 463:339–343.
11. Lee BP, Messersmith PB, Israelachvili JN, Waite JH (2011) Mussel inspired wet adhesives and coatings. *Annu Rev Mater Res* 41:99–132.
12. Holten-Andersen N, et al. (2011) pH-induced metal-ligand cross-links inspired by mussel yield self-healing polymer networks with near-covalent elastic moduli. *Proc Natl Acad Sci USA* 108:2651–2655.
13. Cho SH, Braun PV, White SR (2009) Self-healing polymer coatings. *Adv Mater* 21:645–649.
14. Toohey KS, Sottos NR, Lewis JA, Moore JS, White SR (2007) Self-healing materials with microvascular networks. *Nat Mater* 6:581–585.
15. Balazs AC, et al. (2010) Using nanoparticle-filled microcapsules for site-specific healing of damaged substrates: Creating a "repair-and-go" system. *ACS Nano* 4:1115–1123.
16. Chen X, et al. (2002) A thermally re-mendable cross-linked polymeric material. *Science* 295:1698–1702.
17. Ghosh B, Urban MW (2009) Self-repairing oxetane-substituted chitosan polyurethane networks. *Science* 323:1458–1460.
18. Ayala R, et al. (2011) Engineering the cell-material interface for controlling stem cell adhesion, migration, and differentiation. *Biomaterials* 32:3700–3711.
19. McQueen-Mason S, Cosgrove DJ (1994) Disruption of hydrogen-bonding between plant-cell wall polymers by proteins that induce wall extension. *Proc Natl Acad Sci USA* 91:6574–6578.
20. Colthup NBDL, Wiberley SE (1975) *Introduction to Infrared and Raman Spectroscopy* (Academic, New York), pp 289–325.
21. Barth A, Zscherp C (2002) What vibrations tell us about proteins. *Q Rev Biophys* 35:369–430.
22. Dong J, Ozaki Y, Nakashima K (1997) Infrared, Raman, and near-infrared spectroscopic evidence for the coexistence of various hydrogen-bond forms in poly(acrylic acid). *Macromolecules* 30:1111–1117.
23. Phadke A, Zhang C, Hwang Y, Vecchio K, Varghese S (2010) Templated mineralization of synthetic hydrogels for bone-like composite materials: Role of matrix hydrophobicity. *Biomacromolecules* 11:2060–2068.
24. Lide DR (2009) *Handbook of Chemistry and Physics* (CRC, Boca Raton, FL).